Available online at www.sciencedirect.com

jmr&t
Journal of Materials Research and Technology
https://www.journals.elsevier.com/journal-of-materials-research-and-technology

Original Article

Comparative analysis between normal and submerged friction stir processed friction stir welded dissimilar aluminium alloy joints

*Sipokazi Mabuwa**, *Velaphi Msomi*

Cape Peninsula University of Technology, Mechanical Engineering Department, Cape Town, 7535, South Africa

ARTICLE INFO

Article history:
Received 16 March 2020
Accepted 8 June 2020
Available online 17 July 2020

Keywords:
Microstructural characterization
Microhardness
Surface morphology
Submerged friction stir processing
Normal friction stir processing
Mechanical properties

ABSTRACT

The friction stir welded dissimilar aluminium alloy joints were friction stir processed under air (normal) and underwater (submerged) with room temperature conditions. The joints produced through these two distinct conditions were studied comparatively. The microstructural analysis revealed that due to the water rapid cooling system the grain sizes received were finer compared to the normal friction stir processing ones. The microstructural grain refinement contributed immensely toward the joint tensile properties. The submerged friction stir processed joints were found to be more ductile compared to the normal friction stir processed ones. The positioning of the harder alloy (AA6082) on the advancing side and the soft alloy (AA8011) on the retreating side yielded better results for both normal and submerged conditions. The sampling position was also found to have an impact on the results. This was observed when the specimens cut in the beginning of the joint were studied comparatively with those cut from other locations of the joint.

1. Introduction

The friction stir processing (FSP) technique is a microstructural modification technique derived from friction stir welding principle [1,2]. The FSP technique was developed by Mishra et al. [3] during the year 2000. Ever since then a lot of research work has been produced where FSP was applied on a single surface for different materials and composites [4–8]. Recently the FSP technique has been used to improve the mechanical properties of friction stir welded similar and dissimilar aluminium alloy joints [9,10]. The FSP technique continues to evolve and has also variated to submerged friction stir processing. The submerged friction stir processing (SFSP) works the same way as the FSP, but the whole process takes place with the workpiece immersed under liquid environment [11]. The SFSP is known for its effective cooling which results in ultrafine microstructural grains [12,13]. There are several studies where SFSP was successfully used to modify the microstructure and mechanical properties of aluminium alloy single surfaces.

Sakurada et al. [14] were the first to perform a study on underwater friction joining process for AA6061 proving that enough heat input could be generated to produce sound welds

* *Corresponding author.*
E-mail: sipokazimabuwa@gmail.com (S. Mabuwa).

https://doi.org/10.1016/j.jmrt.2020.06.024

underwater. Since then a lot of work has been reported in the literature under both submerged friction stir welding and submerged friction stir processing. Pang et al. [7] conducted a comparative analysis on-air and underwater FSP using AA7075-T6 plates. The underwater FSP joints had better mechanical properties and the grain sizes were significantly reduced due to the high cooling rate. Similar behavior was noted when comparing the mechanical properties and grain sizes of the normal and submerged conditions on literature [15–20].

Aluminium alloys are mostly preferred as structural materials especially for automotive, marine and aerospace industries. The considered aluminium alloys in this study AA8011 and AA6082-T6 are both applicable in the aerospace industry. There is a big possibility of joining of dissimilar aluminium alloys in the aerospace industry to improve performance. Aluminium alloys remain the most preferred due to a number of reasons like cost-effective and lightweight with outstanding strength.

SFSP is still an emerging technique, although there is a lot of research work done on the topic, however, there are still extensive research areas that still need to be covered. The reason being is that it has been noted that all the literature available only presents SFSP as an ultrafine grain technique to single surface rather than on the prior welded joints. There is no searchable or available literature where SFSP is used on similar or dissimilar friction stir welded joints. This paper reports on the effect of material and specimen positioning of the submerged friction stir processing in comparison to normal friction stir processing of the friction stir welded dissimilar aluminium alloy joints.

2. Experimental setup

The materials used were the dissimilar aluminium alloys AA8011 and AA6082-T6 plates with a thickness of 6 mm. The chemical compositions of the materials are presented in Table 1. Table 2 shows the nominal mechanical properties of the aluminium alloys. The dissimilar joints were fabricated using friction stir welding prior to friction stir processing (FSP). Different material positioning used in this study was as presented in Table 3. The dimensions of the friction stir welded (FSWed) plates (four pairs) were 260 mm × 52 mm. Two pairs of the FSWed plates were fiction stir processed under normal conditions (NFSP) and the other two were friction stir processed underwater or submerged conditions (SFSP). The processing parameters used for NFSP are presented in Table 4. The FSP tool used was made of high-speed steel (HSS) AISI 4140, see Fig. 1(a). The chemical composition of the tool is shown in Table 5.

Table 3 – Material positioning.

Joints	Material positioning	
NFSP FSWed	AA6082–AA8011	AA8011–AA6082
SFSP FSWed	AA6082–AA8011	AA8011–AA6082

Table 4 – FSP parameters.

Parameter	Condition
Tool shoulder diameter	20 mm
Tool probe diameter	7 mm
Tool pin length	5.9 mm
Rotating speed	1100 rpm
Traverse speed	60 mm/min
Dwell time	10 s
Tool plunge depth	5.9 mm
Tool tilt	2°

The submerged friction stir processing fixture was filled with tap water (room temperature). The water head was maintained at 40 mm throughout the whole process. Fig. 1(b) shows the SFSP view. The process parameters used were similar to the NFSP except that the traverse speed of 35 mm/min. The change in traverse speed was due to the observation during trial and error tests, in which a higher traversing speed resulted in a joint with visible defects on the surface. The normal and submerged friction stir processed plates were cut for different tests using the waterjet cutting technology. The cutting method chosen does not temper with the mechanical properties of the specimens.

The tests conducted were the tensile test, microhardness and metallographic analysis. The tensile test specimens were further analyzed for the nature of fracture using a scanning electron microscopy (SEM). The tensile tests were performed using the Instron 8801 with maximum 100 kN load cell. The ASTM-E8M-04 standard was used for the tensile specimen geometry and operating parameters. Fig. 1(c) shows the tensile specimen with dimensions in mm. Data was logged using the Bluehill 3 software. The InnovaTest Falcon 500 machine was used for microhardness testing. The ASTM E384-11 standard was used for Vickers microhardness testing. The 190 HV standard was used for setup. The 0.3 kg load, objective 10× and 20× were used. The 2 mm interval was used from the edge

Table 1 – Chemical compositions [21,22].

	Mg	Zn	Ti	Cr	Si	Mn	Fe	Cu	Al
AA8011	0.28	0.084	0.016	0.028	0.52	0.46	0.74	0.13	Bal
AA6082-T6	0.6–1.2	0.0–0.2	0.0–0.10	0.0–0.20	0.7–1.3	0.0–1.0	0.0–0.5	0.0–0.1	Bal

Table 2 – Mechanical properties of the base materials.

	Ultimate tensile strength (MPa)	Yield strength (MPa)	Elongation (%)	Microhardness (HV)
AA8011	94.1	76	40.17	33.5
AA6082	308	270	25.42	89.6

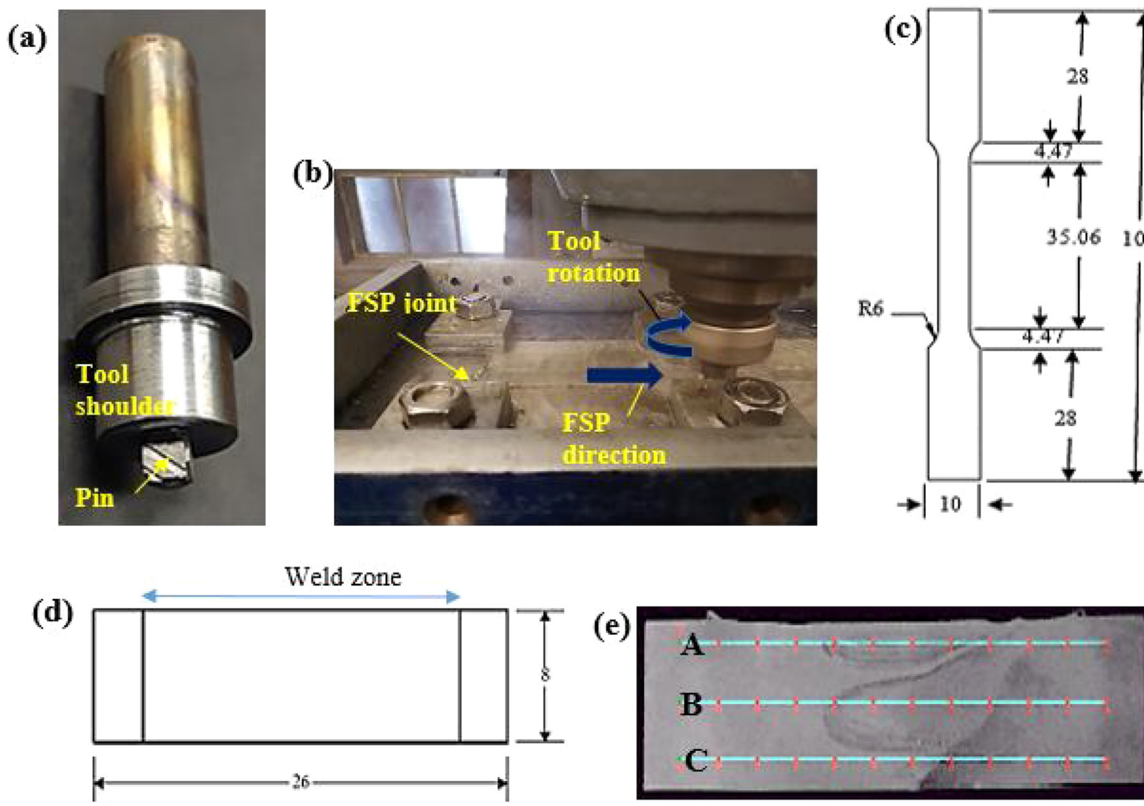

Fig. 1 – (a) FSP tool, (b) SFSP view, (c) tensile test specimen, (d) microhardness specimen and (e) 3-line pattern.

Table 5 – Tool chemical composition [23].

	C	P	Cr	Mo	Mn	Fe	Si	S
AISI 4140	0.38–0.43	0.035	0.80–1.10	0.15–0.25	0.75–1.0	96.79–97.77	0.15–0.30	0.040

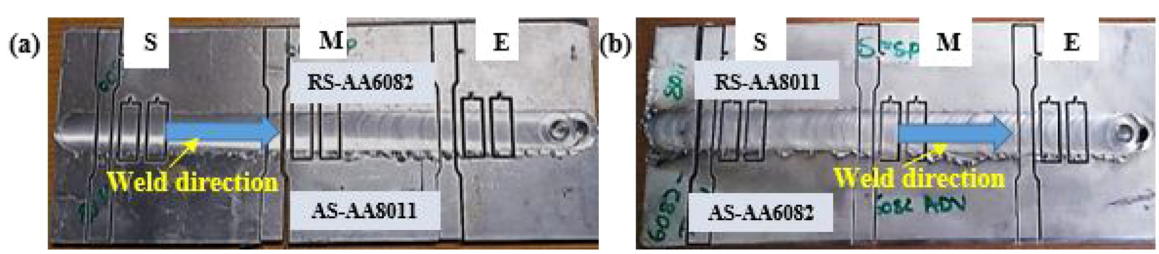

Fig. 2 – Specimen positioning, (a) NFSPed plate and (b) SFSPed plate, (RS – retreating side, AS – advancing side).

to edge (advancing to retreating). The tests were performed along the horizontal section of the welded joint specimen shown in Fig. 1(d). The 3-line pattern format as depicted in Fig. 1(e) was used for all the specimens tested, where A stands for the line at the top, B for the line in the middle and C for the line at the bottom of the specimen. The metallographic analysis was performed using the Motic AE2000 microscope. The cross-sections surface of the welds were grinded, polished then etched using the modified Keller's reagent (10 ml HNO_3, 1.5 ml HCL, 1.0 ml HF and 87.5 ml distilled H_2O) and Weck's reagents (1 g NaOH, 4 g $KMnO_4$ and 100 ml distilled H_2O). Fig. 2 shows the locations where the specimens were extracted. The labels S, M and E were used to mark the start, middle and the end weld respectively.

3. Results and discussion

3.1. *Metallographic analysis*

Fig. 3.1 (a) and (b) show the macrographs for the friction stir welded joints before the processing. The normal friction stir processed macrographs are shown in Fig. 3.1(c) to (h), with (c) to (e) for AA6082 on the advancing side and (f) to (h) for AA8011 on the advancing side. Fig. 3.1(i) to (k) show the macrographs for the submerged friction stir processed joints where AA6082 was positioned on the advancing side and (l) to (n) for AA8011 on the advancing side. There are defects that were observed in some stir zones [(c), (d), (f), (g) and(l)] and these

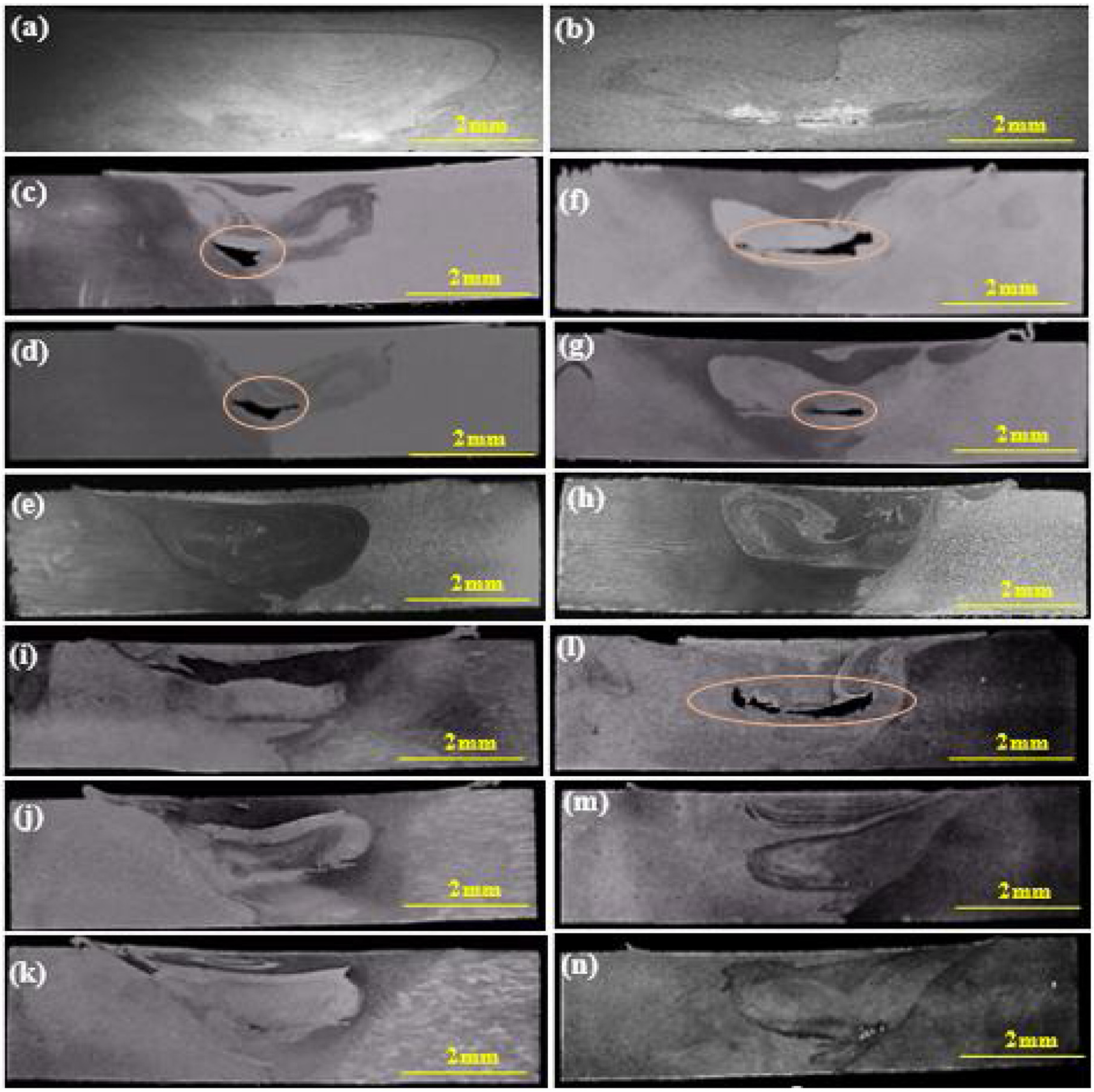

Fig. 3.1 – Macrographs; (a) FSW-AA6082 on AS, (b) FSW-AA8011 on AS; NFSP-AA6082 on AS: (c) Start, (d) Middle, (e) End; AA8011 on AS: (f) Start, (g) Middle, (h) End; SFSP-AA6082 on AS: (i) Start, (j) Middle, (k) End; SFSP AA8011 on AS: (l) Start, (m) Middle and (n) End.

defects are normally attributed toward insufficient material flow which originates from an inadequate heat input [24–27]. The rest of the macrographs showed structures with onion rings with no defects which means that the joint experienced adequate heat input which resulted to sufficient material flow [28–30]. The heat experienced during the processing differed for each region (start, middle and toward the end of the joint). It was also observed that defects dominate on the joints that were produced from NFSP and mostly specimens that were extracted from the beginning of the weld. There is no trace of such defects with samples produced from SFSP beside one that was extracted at the beginning of the weld when AA8011 was placed on the advancing side. These macrograph results do depict the impact of SFSP on joint quality.

The microscopic view of the joints and their respective base materials are presented in Fig. 3.2 . Fig. 3.2(a) presents the AA6082 base material with and average grain size of 33.3 μm and (b) shows the AA8011 base material with an average grain size of 22.93 μm. The microstructural grain arrangement of the joint produced by varying the material positioning during FSW is illustrated in Fig. 3.2(c) and (d). The positioning of AA6082 on the advancing side resulted in FSWed joint having mean grain diameter of about 8.25 μm whereas the mean grain diameter of 9.97 μm was measured on all specimens where AA8011 was placed on the advancing side. Fig. 3.2(e) to (g) shows the NFSP-AA6082 on the advancing side and (h) to (j) shows the NFSP-AA8011 on the advancing side. The SFSP micrographs with AA6082 on the advancing side are shown in Fig. 3.2(k) to (m). Fig. 3.2 (n) to (p) presents the joint micrographs produced when AA8011 was placed on the advancing side.

The average grain size for NFSP joint with AA8011 positioned on the advancing side (AA8011A) was about 6.18 μm

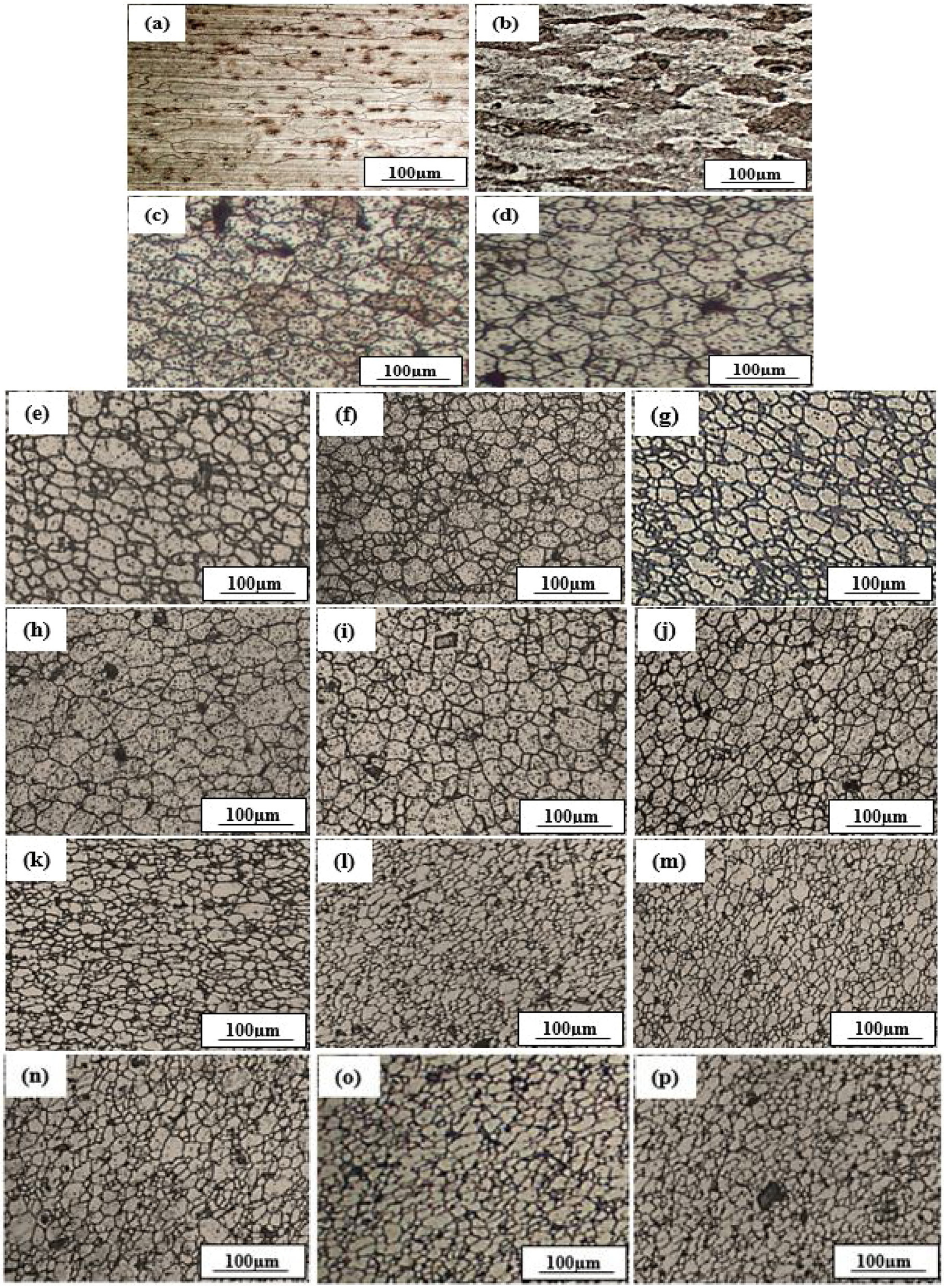

Fig. 3.2 – Micrographs at objective 5× (a) AA6082 base material, (b) AA8011 base material; at objective 50×, (c) FSW-AA6082 on AS, (d) FSW-AA8011 on AS; NFSP-AA6082 on AS: (e) Start, (f) Middle, (g) End; AA8011 on AS: (h) Start, (i) Middle, (j) End; SFSP-AA6082 on AS: (k) Start, (l) Middle, (m) End; SFSP AA8011 on AS: (n) Start, (o) Middle and (p) End.

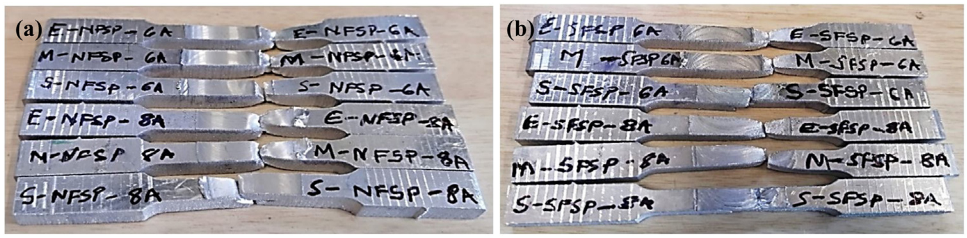

Fig. 4.1 – Post tensile specimens, (a) NFSP and (b) SFSP.

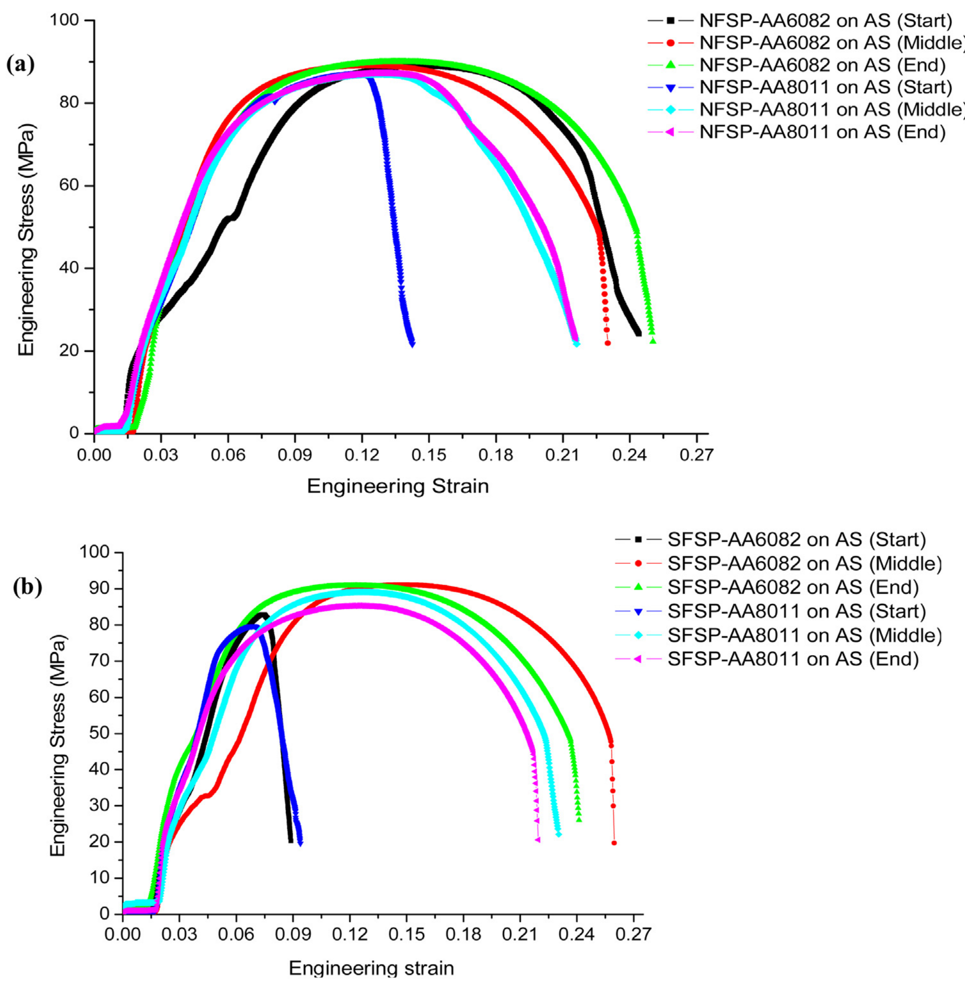

Fig. 4.2 – Tensile stress–strain curves, (a) NFSP and (b) SFSP.

whereas placing AA6082 on the advancing side yielded an average grain size of about 5.15 μm. The average grain size for SFSP joint when AA8011 was positioned on the advancing side was 3.22 μm whereas an average grain size of 2.76 μm was obtained when AA6082 was positioned on the advancing side. The grain refinement during both SFSP/NFSP is due to the re-stirring and dynamic re-recrystallization which occurred during both conditions on the FSWed joints [9,10]. The results distinctively revealed that placing AA6082 on the advancing side and AA8011 on the retreating side yielded finer grains compared to when AA8011 was on the advancing side. This reaction was due to the materials being properly mixed and the joint experiencing adequate heat and material flow which occurs mostly when the harder alloy is placed on the advancing side [33,34]. Additionally, in both said conditions it was noted that when it comes to the specimen positioning, the specimens cut toward the middle and the end had better results in comparison to the ones cut at the beginning of the joints. This behavior is influenced by the quality of the weld in which in the case of specimens' M and E showed no defects. The microscopic behavior observed in this study is very consistent with the behavior reported in the literature [7,10,12,29,31,32].

3.2. *Tensile tests*

Fig. 4.1 (a) shows the post tensile specimens for NFSP and (b) for SFSP with visible fracture locations. In both conditions, the

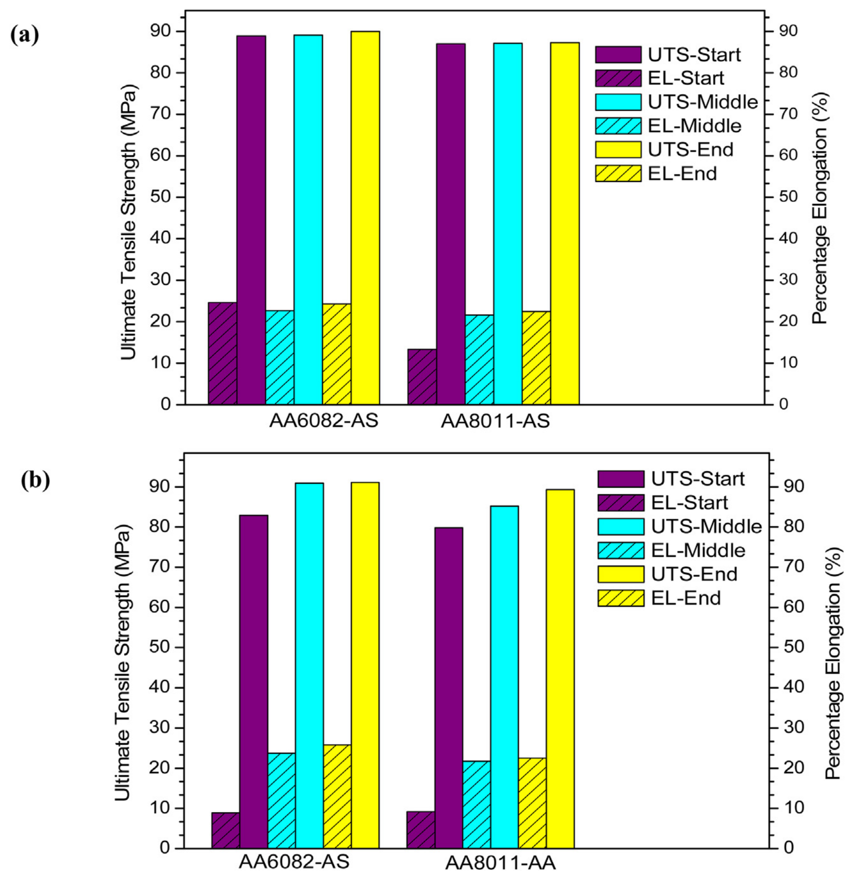

Fig. 4.3 – Ultimate tensile stress-elongation bar charts, (a) NFSP and (b) SFSP.

failure occurred on the AA8011 (weaker alloy) side regardless of heat-affected zone (HAZ) and stir zone (SZ). The specimens that were cut at the starting position of the joint where AA8011 was positioned at the advancing and AA6082 at the retreating side had defects in both NFSP and SFSP. This behavior was due to inadequate heat generation [24,25]. The same phenomenon was noted on the macrographs of the same position. This defect weakens the joint hence these specimens failed toward the center of the SZ. The specimens cut at the middle and end of the joint consistently failed at the HAZ when AA6082 was positioned on the advancing side. All other specimens failed at thermos-mechanically affected zone (TMAZ) when AA8011 was positioned on the advancing side. This behavior was observed for both NFSP and SFSP specimens.

The FSWed joints prior NFSP/SFSP had a maximum ultimate tensile stress (UTS) of 92.9 MPa and percentage elongation of 26.68% when AA6082 was positioned on the advancing side. The maximum UTS of 60.9 MPa and percentage elongation of 24.54% were attained when AA8011 was placed on the advancing side. Fig. 4.2 (a) and (b) illustrates the stress–strain curves of the NFSP and SFSP, respectively. The difference in processing conditions had a notable effect on the tensile strength of the specimens. Fig. 4.3 (a) and (b) presents the UTS-elongation bars charts of the joints being compared. The specimens at the start of the joint all have lower strengths and the ones toward the end have the maximum strengths. This is strength variation is attributed to heat experienced by the joint during both SFSP/NFSP as well as the grain structure associated with the respective positions [35]. The SFSP had the maximum tensile strength of 91.1 MPa and 89.2 MPa for AA6082 on the advancing side and AA8011 on the advancing side, respectively. The NFSP had a maximum tensile strength of 90 MPa for AA6082 on the advancing side and 87.3 MPa for AA8011 on the advancing side.

The SFSP joints possessed higher UTS compared to NFSP. The UTS enhancement observed in this work is similar to the one reported in the literature [36–38]. The NFSP had a maximum percentage elongation of 24.62% when AA6082 was positioned on the advancing side and 21.65% when AA8011 was positioned on the advancing side. The highest percentage elongation of 28.7% was achieved when AA6082 was positioned on the advancing side during SFSP whereas 22.5% was achieved when AA8011 was positioned on the advancing side. In most case, the increase in UTS results in decrease in percentage elongation and the visa versa [9,10]. The results shown in Fig. 4.3 (b) has shown the opposite to this normalcy. This behavior suggests that SFSP can be used in the enhancement of both UTS and percentage elongation of the joint.

3.3. *Fracture surface morphology*

Fig. 5.1 shows the fractured surface morphologies of the normal friction stir processed friction stir welded dissimilar aluminium joints. The fractured surfaces presented in Fig. 5.1(a)–(c) shows the specimens cut at the start, middle

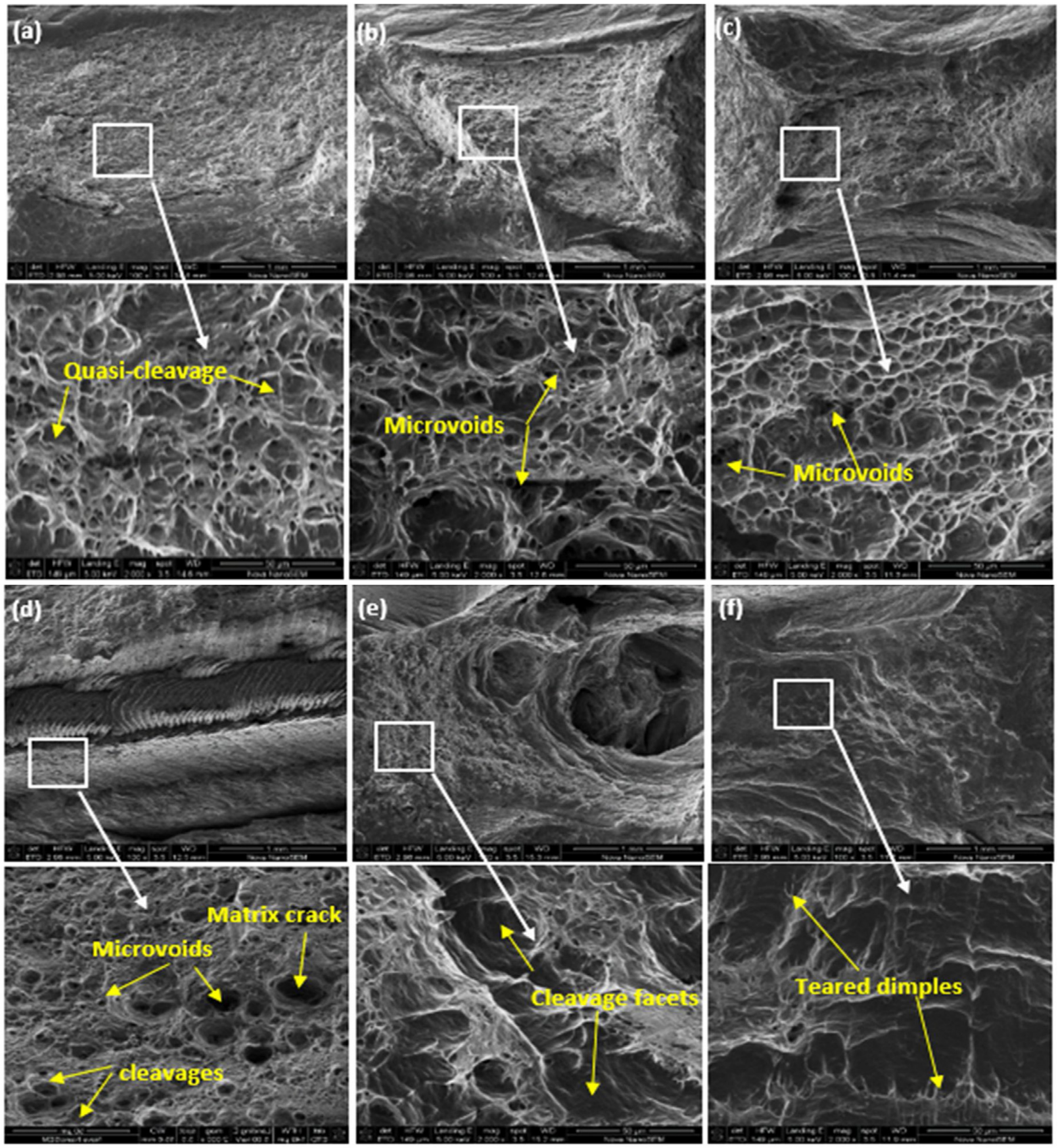

Fig. 5.1 – NFSP fractographs, AA6082 on AS (a) Start, (b) Middle, (c) End; AA8011 on AS (d) Start, (e) Middle and (f) End.

and the end of the weld where AA6082 was positioned on the advancing side during NFSP. All the mentioned specimens revealed a ductile failure morphology which is characterized by the presence of the microvoids, quasi-cleavages and dimples [39,40]. Fig. 5(d)–(f) show specimens cut at the start, middle and the end of the weld where AA8011 was positioned on the advancing side. Fig. 5.1(d) shows a ductile failure morphology with microvoids, cleavages and matrix crack. Fig. 5.1(e) and (f) show dimples that are interlaced with quasi-cleavage morphology [41]. This phenomenon shows that after the re-heating and re-stirring during the NFSP the joint plasticity was reduced [9,10].

The submerged friction stir processed friction stir welded dissimilar aluminium joints surface morphologies are depicted in Fig. 5.2 . Fig. 5.2(a), (b) and (c) shows the specimens cut at the start, middle and end of the weld. All the specimens consisted of similar ductile features like cleavage facets, microvoids, and matrix cracks [9,40,41]. The specimens where AA6082 was positioned on the advancing side consisted of fine homogeneous dimples regardless of the specimen position. The specimens with AA8011 on the advancing side showed an irregular dimple pattern where the specimen cut at the start had coarse dimples while the fine dimples were noted on the specimen cut at the end of the weld. This behavior is a result of the microstructural grains changes across the joint which was depending on the heat and material flow experienced during the SFSP process [35,39–42]. The SFSP and the NFSP fractographs all showed ductile behavior with the SFSP showing more uniform patterns, especially where the AA6082 was on the advancing side.

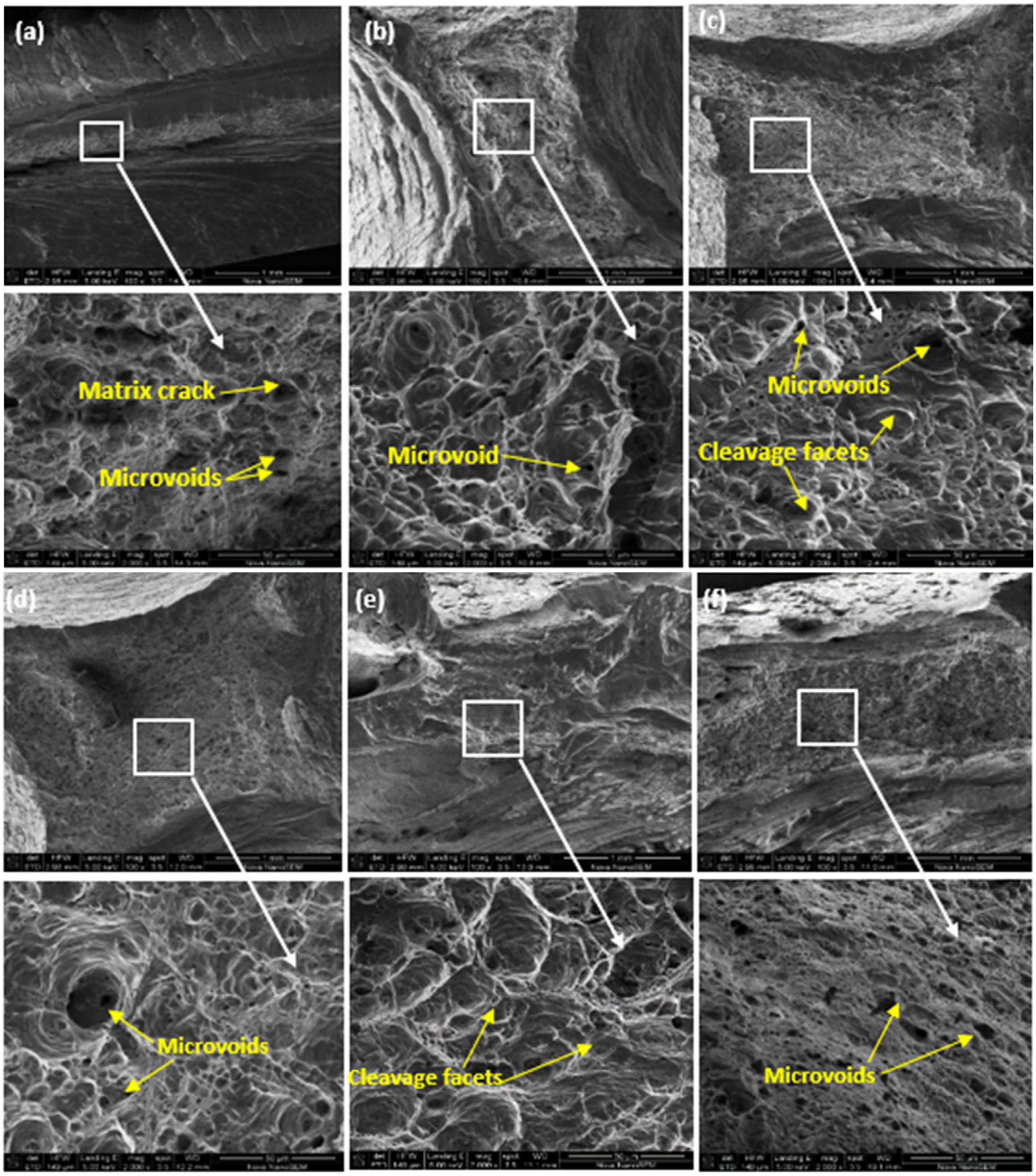

Fig. 5.2 – SFSP fractographs AA6082 on AS (a) Start, (b) Middle, (c) End; AA8011 on AS (d) Start, (e) Middle and (f) End.

3.4. *Microhardness*

The maximum microhardness of the FSWed joint where AA6082 was positioned on the advancing side was ~74 HV whereas ~62 HV was measured when AA8011 on the advancing side. The Vickers microhardness profiles of the NFSP are shown in Fig. 6.1 . An approximate microhardness of ~90 HV was obtained when AA6082 was position on the advancing side during NFSP and this was higher compared to that of the FSWed one. The increase in hardness was a result of the complete solution and the new precipitation in the stir zone [34]. The microhardness of ~55 HV was obtained with AA8011 on the advancing side which is lower than that of the FSWed joint with same material positioning. During the submerged friction stir processing, the positioning of AA6082 on the advancing side resulted in the microhardness of ~60 HV as shown in Fig. 6.2 , which is lower compared to the NFSP one and the FSWed one of the same material positioning. The microhardness of ~45 HV was obtained when AA8011 was positioned on the advancing side, also lower than the NFSP and the FSWed one. This behavior in the microhardness of the underwater conditions is due to strain hardening of the low-density dislocations, precipitates distribution and the reduced microstructural grain size [24,42–45]. When AA6082 was placed on the advancing side during both NFSP and SFSP the microhardness decreased from the stir

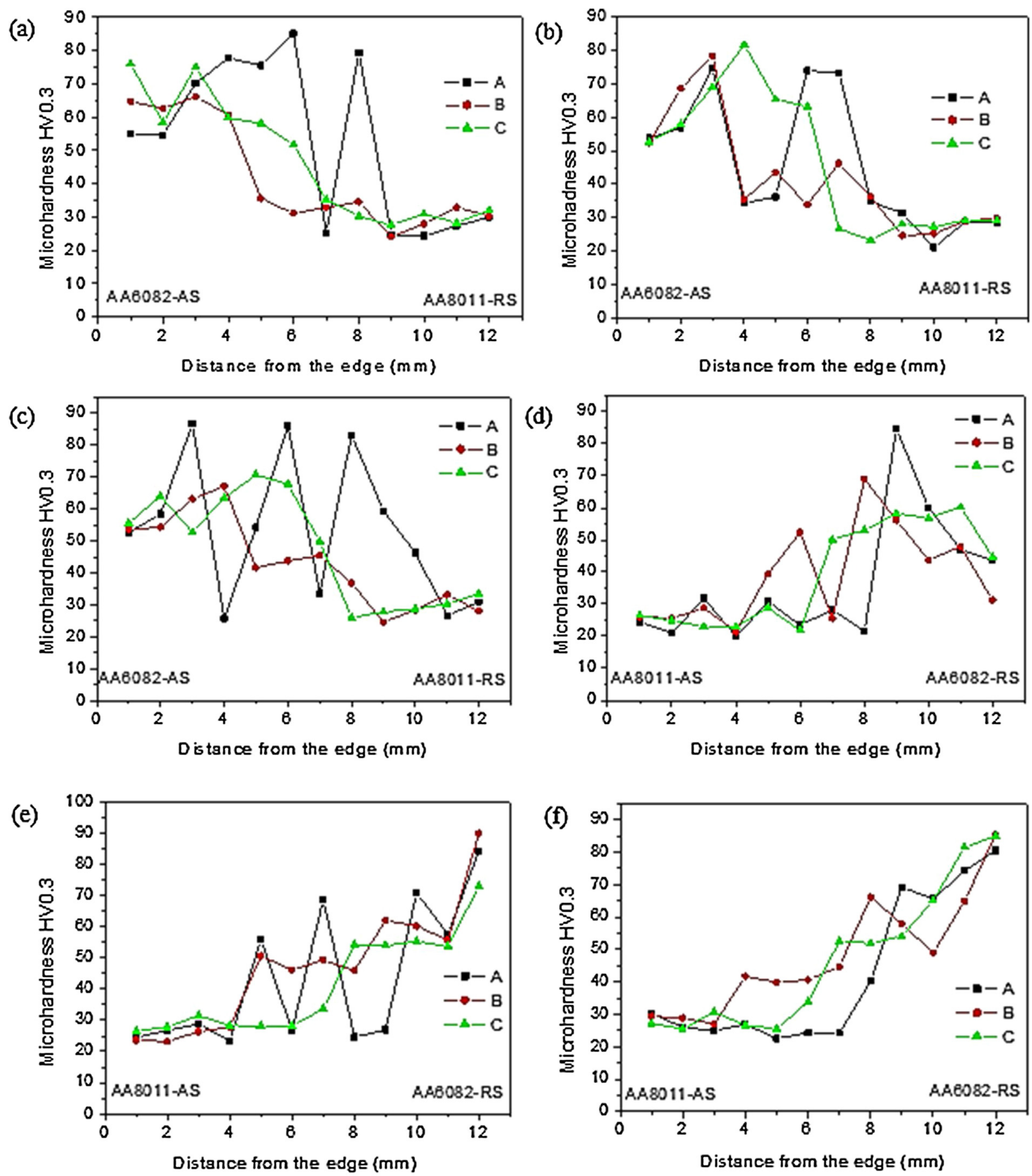

Fig. 6.1 – NFSP microhardness profiles, AA6082 on AS (a) Start, (b) Middle, (c) End; AA8011 on AS (d) Start, (e) Middle and (f) End.

zone to the AA8011 side. Additionally, when AA8011 was placed on the advancing side the microhardness increase to the AA6082 side. Specimen positioning had a negligible impact on the microhardness of the stir zone for both NFSP and SFSP joints.

4. Conclusions

The friction stir welded dissimilar aluminium alloy joints were successfully friction stir processed under two unique conditions i.e. air (normal) and underwater (submerged). It should

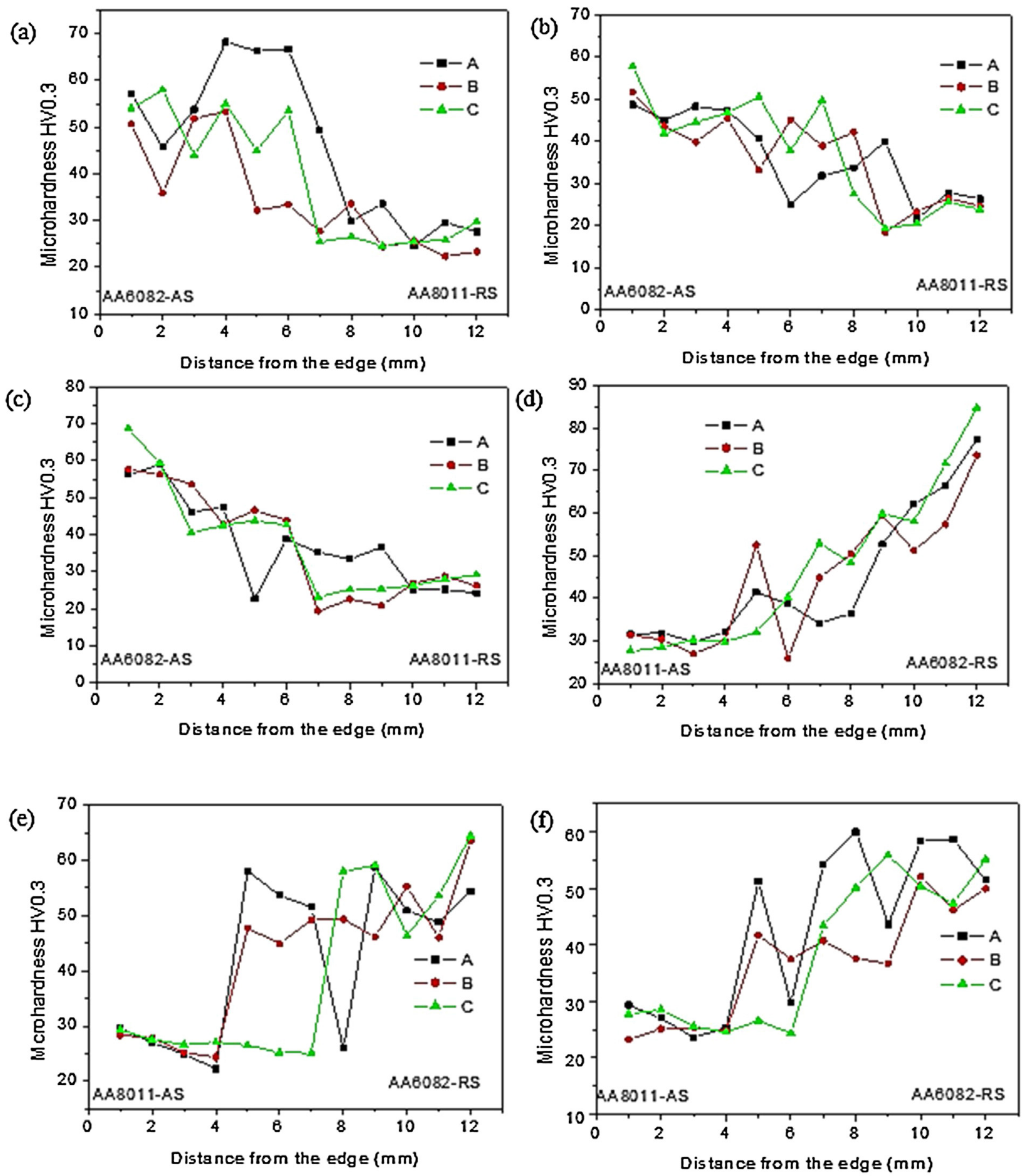

Fig. 6.2 – SFSP microhardness profiles, AA6082 on AS (a) Start, (b) Middle, (c) End; AA8011 on AS (d) Start, (e) Middle and (f) End.

be noted due to no available literature on SFSP and NFSP of friction stir welded dissimilar joints, the obtained results were referenced to SFSP and NFSP of the single surface materials as well as SFSW. Based on the results of this study, the following conclusion can be drawn:

- The SFSP technique played a significant role in the grain refinement compared to the NFSP technique and this is linked to cooling rate that is facilitated by water.
- The submerged friction stir processed joints were found to be more ductile than the normal friction stir processed ones.
- The SFSP technique produced joints with an improved tensile properties than those produced by NFSP. It was also observed that SFSP can be used as the mechanism of enhancing the joint's UTS and percentage elongation
- The fractographic analysis correlated with the tensile results that both NFSP and SFSP of the friction stir welded dissimilar joints results in a ductile fracture and the SFSP

being the most ductile ones for the specimen cut toward the end of the joint (AA6082 on the advancing side).

- The materials positioning also plays a significant role toward the strength of the joint on both processing conditions i.e. NFSP and SFSP.
- The specimen positioning was also found to have an impact on the results and this was observed with lower properties of all the specimens cut at the start of the processed joints against specimens cut from other locations on both processing conditions.

Conflict of interests

The authors declare no conflict of interest in this study.

Funding

The authors would like to acknowledge the National Research Foundation (NRF) Thuthuka Grant for funding this study.

Data availability

Additional data available upon request.

Authors' contribution

V. M. conceived the research and provided guidance. S. M. and V. M. did the experiments. S. M. wrote the manuscript. S. M. and V. M. contributed to the scientific discussions. All authors reviewed the manuscript.

Acknowledgements

The authors would like to acknowledge the Cape Peninsula University of Technology mechanical engineering workshop staff especially Miss S. Petersen for her assistance in specimen preparation. Special appreciation also goes Miranda Waldron from the University of Cape Town for assistance with scanning electron microscopy tests.

REFERENCES

[1] Mishra RS, Mahoney MW, McFadden SX, Mara NA, Mukherjee AK. Scr Mater 2000;42:163–8.
[2] Mishra RS, Mahoney MW. Mater Sci Forum 2001;357–359:507–12.
[3] Ma Z. Friction stir processing technology: a review. Metall Mater Trans A 2008;39:642–58.
[4] Kurt A, Uygur I, Cete E. Surface modification of aluminium by friction stir processing. J Mater Process Technol 2011;211(3):313–7.
[5] Sudhakar M, Srinivasa Rao CH, Meera Saheb K. Production of surface composites by friction stir processing – a review. Mater Today Proc 2018;5(1):929–35.
[6] Maamoun AH, Veldhuis SC, Elbestawi M. Friction stir processing of AlSi10Mg parts produced by selective laser melting. J Mater Process Technol 2019;263:308–20.
[7] Pang JJ, Liu FC, Liu J, Tan MJ, Blackwood DJ. Friction stir processing of aluminum alloy AA7075: microstructure, surface chemistry and corrosion resistance. Corros Sci 2016;106:217–28.
[8] Orozco-Caballero A, Alvarez-Leal M, Hidalgo-Manrique P, Cepeda-Jimenez CM, Ruano OA, Carreno F. Grain size versus microstructural stability in the high strain rate superplastic response of a severely friction stir processed Al-Zn-Mg-Cu alloy. Mater Sci Eng A 2017;680:329–37.
[9] Mabuwa S, Msomi V. The effect of friction stir processing on the friction stir welded AA1050-H14 and AA6082-T6 joints. Mater Today Proc 2019, http://dx.doi.org/10.1016/j.matpr.2019.10.039. ISSN: 2214-7853.
[10] Mabuwa S, Msomi V. Effect of friction stir processing on gas tungsten arc-welded and friction stir-welded 5083-H111 aluminium alloy joints. Adv Mater Sci Eng 2019:1–15.
[11] Albakr AN, Aljoaba SZ, Khraisheh MK. Modelling of friction stir processing with in-process cooling using computational fluid dynamics analysis. Adv Sustainable Manuf 2011:99–105.
[12] Feng X, Liu H, Lippold CJ. Microstructure characterization of the stir zone of submerged friction stir processed aluminum alloy 2219. Mater Charact 2013;82:97–102.
[13] Liu HJ, Feng XL. Effect of post-processing heat treatment on microstructure and microhardness of water-submerged friction stir processed 2219-T6 aluminum alloy. Mater Des 2013;47:101–5.
[14] Sakurada D, Katoh K, Tokisue H. Underwater Friction welding of 6061 aluminum alloy. JILM 2002;52:2–6.
[15] Hoffman DC, Kennesh SV. Submerged friction stir processing (SFSP): an improved method for creating ultra-fine-grained bulk materials. Mater Sci Eng A 2005;402(1–2):234–41.
[16] Rathinasuriyan C, Senthil Kumar VS. Modelling and optimization of submerged friction stir welding parameters for AA6061-T6 alloy using RSM. Kov Mater 2016;54:297–304.
[17] Mofid MA, Abdollah-Zadeh A, Ghaini FM, Gu CH. Submerged friction-stir welding (SFSW) underwater and under liquid nitrogen: an improved method to join Al alloys to Mg alloys. Metall Mater Trans A 2012;43:5106–14.
[18] Zhang HJ, Liu H, Yu L. Microstructure and mechanical properties as a function of rotation speed in underwater friction stir welded aluminum alloy joints. Mater Des 2011;32:4402–7.
[19] Mofid MA, Abdollah-zadeh A, Malek Ghaini F. The effect of water cooling during dissimilar friction stir welding of Al alloy to Mg alloy. Mater Des 2012;36:161–7.
[20] Chai F, Zhang D, Yuanyuan L, Zhang W. High strain rate superplasticity of a fine-grained AZ91 magnesium alloy prepared by submerged friction stir processing. Mater Sci Eng A 2013;568:40–8.
[21] Selvaraj G, Karthikeyan T, Mohanadass R, Indhumath S. Investigation on mechanical properties of welded aluminium joints of aa 8011 using friction stir welding. Int J Appl Eng Res 2015;10(13):11095–100.
[22] Braga DFO, de Sousa LMC, Infante V, da Silva LFM, Moreira PMG. Aluminium friction stir weld-bonded joints. J Adhes 2016;92(7–9):665–78.
[23] Aslan E, Camuşcu N, Birgören B. Design optimization of cutting parameters when turning hardened AISI 4140 steel (63 HRC) with Al_2O_3 + TiCN mixed ceramic tool. Mater Des 2007;28(5):1618–22.
[24] Chandrana R, Santhanam SKV. Submerged friction stir welding of 6061-T6 aluminium alloy under different water heads. Mater Res 2018;21(6):1–12.
[25] Vignesh VR, Padmanaban R, Datta M. Influence of FSP on the microstructure, microhardness, intergranular corrosion susceptibility and wear resistance of AA5083 alloy. Tri Mater Surf Interf 2018;12(3):157–69.

[26] Baghdadi AH, Selamat NFM, Sajuri Z. Effect of tool offsetting on microstructure and mechanical properties dissimilar friction stir welded Mg-Al alloys. IOP Conf Ser Mater Sci Eng 2017;238(012018):1–10.
[27] Luo X, Fang D, Li Q, Chai Y. Microstructure and mechanical properties of An Mg-4.0 Sm-1.0 Ca alloy during thermomechanical treatment. J Rare Earths 2016;34(11):1134–8.
[28] Ramaiyan S, Santhanam SKV, Muthuguru P. Effect of scroll pin profile and tool rotational speed on mechanical properties of submerged friction stir processed AZ31B magnesium alloy. Mater Res 2018;21(3):e20170769, 1–9.
[29] Chai F, Zhang F, Li Y, Zhang W. High strain rate super plasticity of a fine-grained AZ91 magnesium alloy prepared by submerged friction stir processing. Mater Sci Eng A 2013;568:40–8.
[30] Huang G, Wu J, Hou W, Shen Y. Microstructure, mechanical properties and strengthening mechanism of titanium particle reinforced aluminum matrix composites produced by submerged friction stir processing. Mater Sci Eng A 2013;34:353–63.
[31] Su JQ, Nelson TW, Sterling CJ. Grain refinement of aluminum alloys by friction stir processing. Philos Mag 2006;86(1):1–24.
[32] Darras B, Kishta E. Submerged friction stir processing of AZ31 Magnesium alloy. Mater Des 2013;47:133–7.
[33] Park SK, Hong ST, Park JH, Park KY, Kwon YJ, Son HJ. Effect of material locations on properties of friction stir welding joints of dissimilar aluminium alloys. Sci Technol Weld Joining 2010;15(4):331–6.
[34] Cavaliere P, De Santis A, Panella F, Squillace A. Effect of welding parameters on mechanical and microstructural properties of dissimilar AA6082–AA2024 joints produced by friction stir welding. Mater Des 2009;30:609–16.
[35] Msomi V, Mbana N. Mechanical properties of friction stir welded AA1050-H14 and AA5083-H111 joint: sampling aspect. Metals 2020;10(214):1–17.
[36] Derazkola HA, Eyvazian A, Simchi A. Submerged friction stir welding of dissimilar joints between an Al-Mg alloy and low carbon steel: thermo-mechanical modeling, microstructural features, and mechanical properties. Manuf Process 2020;50:68–79.
[37] Huang G, Wu J, Hou W, Shen Y. Microstructure, mechanical properties and strengthening mechanism of titanium particle reinforced aluminum matrix composites produced by submerged friction stir processing. Mater Sci Eng A 2018;734:353–63.
[38] Chandran R, Santhanam SKV. Submerged friction stir welding of 6061-T6 aluminium alloy under different water heads. Mater Res 2018;21(6):e20171070, 1–12.
[39] Yan Y, Li H, Zhang J, Kong N. The effect of initial annealing microstructures on the forming characteristics of Ti-4Al-2V. Titanium Alloy Met 2019;9(5):576, 1–12.
[40] Zhao HJ, Wang BY, Liu G, Yang L, Xiao WC. Effect of vacuum annealing on microstructure and mechanical properties of TA15 titanium alloy sheets. Trans Nonferr Met Soc China 2015;25:1881–8.
[41] Liu JH, Huang CX, Wu SD, Zhang ZF. Tensile deformation and fracture behaviors of high purity polycrystalline zinc. Mater Sci Eng A 2008;490:117–25.
[42] Chen YC, Nakata K. Effect of the surface state of steel on the microstructure and mechanical properties of dissimilar metal lap joints of aluminum and steel by friction stir welding. Scr Mater 2007;58:433–6.
[43] Cao X, Jahazi M. Friction stir welding of dissimilar Al/Al and Al/non-Al Alloys: a review. Adv Manuf Technol 2009;56:370–6.
[44] Xue P, Xiao B, Ma Z. Achieving large-area bulk ultrafine grained Cu via submerged multiple-pass friction stir processing. Mater Sci Technol 2013, http://dx.doi.org/10.1016/j.jmst.2013.09.021.
[45] Liu H, Zhang H, Huang Y, Yu L. Mechanical properties of underwater friction stirwelded 2219 aluminum alloy. Trans Nonferr Met Soc China 2010;20:1387–91.